Journal of Materials Chemistry

Dynamic Article Links

Cite this: *J. Mater. Chem.*, 2011, **21**, 13926

www.rsc.org/materials

PAPER

Self-assembly of layered double hydroxide nanosheets/Au nanoparticles ultrathin films for enzyme-free electrocatalysis of glucose†

Jingwen Zhao, Xianggui Kong, Wenying Shi, Mingfei Shao, Jingbin Han, Min Wei,* David G. Evans and Xue Duan

Received 10th May 2011, Accepted 6th July 2011
DOI: 10.1039/c1jm12060c

This paper reports the fabrication of layered double hydroxide nanosheets (LDH nanosheets)/Au nanoparticles (AuNPs) ultrathin films (UTFs) *via* the layer-by-layer (LBL) assembly technique, and their electrocatalytic performance for the oxidation of glucose was demonstrated. UV-vis absorption spectra show the uniform growth of the UTFs and the enhancement of interlayer plasmon coupling of AuNPs upon increasing deposition cycle. The XRD results indicate that the $(LDH/AuNPs)_n$ UTFs possess long-range order stacking in the normal direction of the substrate, with AuNPs accommodated between the LDH nanosheets as a monolayer arrangement. SEM, TEM and AFM images reveal a high dispersion of AuNPs on the surface of the LDH nanosheets without aggregation. The electrochemical behavior of the UTF modified fluorine-doped tin oxide (FTO) electrode was studied by cyclic voltammetry and electrochemical impedance spectroscopy. The $(LDH/AuNPs)_n$ UTF shows improved electron transfer kinetics, owing to the formation of electron tunneling junctions resulting from the interlayer plasmon coupling. This leads to new channels for facilitating electron transfer within the UTFs. In addition, the $(LDH/AuNPs)_8$ electrode displays significant electrocatalytic performance for glucose with a linear response range (50 μM–20 mM), low detection limit (10.8 μM), high sensitivity (343 μA mM^{-1} cm^{-2}), good stability and reproducibility. Therefore, this work provides a feasible method to immobilize metal nanoparticles using the LDH nanosheet as a 2D matrix, which is promising for the development of enzyme-free sensors.

1. Introduction

Electrocatalytic oxidation of glucose has attracted much interest over past years for the construction of glucose-oxygen biofuel cells,[1] abiotically catalyzed fuel cells,[2] especially for the development of glucose sensing in human blood which has long been recognized as an important clinical test for diagnosing diabetes mellitus.[3] Biosensors with high selectivity and sensitivity for glucose based on the corresponding oxidases or other enzymes have been reported.[4] However, such sensors usually suffer from long-term stability due to the intrinsic nature of enzymes.[5] Therefore, considerable attention has been focused on direct electrocatalytic oxidation of glucose at noble metal-based[6] and alloys-based[7] electrodes for the purpose of achieving enzyme-free sensing with fast amperometric response, high stability and reproducibility.

Gold as an attractive material for the oxidation of glucose has been extensively studied in the field of electrocatalysis, electroanalysis and biosensors due to its stable chemical properties, good biocompatibility, high catalytic activity and, more importantly, no observable surface poisoning during the electrochemical process compared with other metals.[8] To date, several nanofabrication techniques have been applied for the assembly or incorporation of AuNPs into the desired 2D or 3D nanostructures for the fabrication of electronic and electrochemical devices.[9,10] The layer-by-layer (LBL) assembly method was commonly used to tailor the composition, thickness and architecture of AuNPs-based films by using polyelectrolytes,[17b] bifunctional molecules[9a] and biomolecules[4b] as cross-linkers. In these cases unfortunately, the aggregation of AuNPs is normally inevitable due to the disordered morphology and the intertwist of the cross-linkers, which lead to decreases in the utilization of AuNPs active sites and the resulting catalytic and electrocatalytic efficiency.[11] Therefore, it is of crucial importance to develop new approaches to obtain well-organized structures with highly dispersed AuNPs in a suitable matrix which can provide a stable microenvironment for electron transfer.

Layered double hydroxides (LDHs), whose formula can be generally expressed as $[M^{2+}_{1-x}M^{3+}_{x}(OH)_2]^{x+}[A^{n-}_{x/n}]^{x-}\cdot mH_2O$ (M^{2+} and M^{3+} represent di- and tri-valent metal cations, respectively; A^{n-} is an n-valent anion), are a class of two-dimensional layered materials.[12] Based on the attractive features including intercalation property, non-toxicity, high stability and

State Key Laboratory of Chemical Resource Engineering, Beijing University of Chemical Technology, Beijing, 100029, China. E-mail: weimin@mail.buct.edu.cn; Fax: +86-10-64425385; Tel: +86-10-64412131

† Electronic supplementary information (ESI) available. See DOI: 10.1039/c1jm12060c

biocompatibility, LDH materials play a vital role as a host matrix in the fields of catalysis, biology, optical devices and electrochemical sensors.[13] Recently, LDHs have been exfoliated into positively charged nanosheets with the ultimate 2D anisotropy which are favorable for assembly into functional multilayer nanostructures by employing an LB or LBL technique.[14] This therefore enlightens us to fabricate the electrochemical sensor by the alternating assembly of positively charged LDH nanosheets and negatively charged AuNPs on fluorine-doped tin oxide (FTO) electrodes using the LBL approach, in which the LDH nanosheets serve as both building block and cross-linker. In contrast to previous studies with polyelectrolytes or bifunctional molecules as cross-linkers, the use of LDH nanosheets offers several advantages: firstly, the LDH nanosheets provide a confined and stable microenvironment for the immobilization of AuNPs with a long range order stacking; secondly, the uniform dispersion of positive charge in the LDH nanosheets will result in a high dispersion of AuNPs particles and suppress their aggregation. Moreover, the film component and thickness can be precisely controlled in the nanometre scale with simple manipulation and versatility.

In this work, positively charged LDH nanosheets as building blocks were assembled alternately with negatively charged AuNPs on the FTO substrate *via* the electrostatic LBL deposition technique (Scheme 1). The obtained $(LDH/AuNPs)_n$ UTFs show a long-range ordered structure in which highly dispersed AuNPs were obtained. The formation of electron tunneling junctions due to the interlayer plasmon coupling of AuNPs facilitates the electron transfer throughout the UTFs. Moreover, the modified electrode displays remarkable electrocatalytic performance towards the oxidation of glucose with high sensitivity, low detection limit as well as long-term stability. The results demonstrate that LDH nanosheets can serve as one promising material for the immobilization of metal particles which can be potentially applied in the fields of electrocatalysis and electrochemical sensors.

2. Experimental section

2.1 Materials

Hydrogen tetrachloroaurate hydrate ($HAuCl_4 \cdot 3H_2O$, >99.9%) was purchased from Aldrich Co. Ltd. Poly(styrenesulfonic acid) (PSS, MW = 70 000) was obtained from Alfa Aesar Chemical Co. Ltd. Analytical grade chemicals including $Zn(NO_3)_2 \cdot 6H_2O$, $Al(NO_3)_3 \cdot 9H_2O$ and urea were used without further purification. Deionized water from a Milli-Q Millipore system (>18.0 MΩ cm) was used in all the experimental processes.

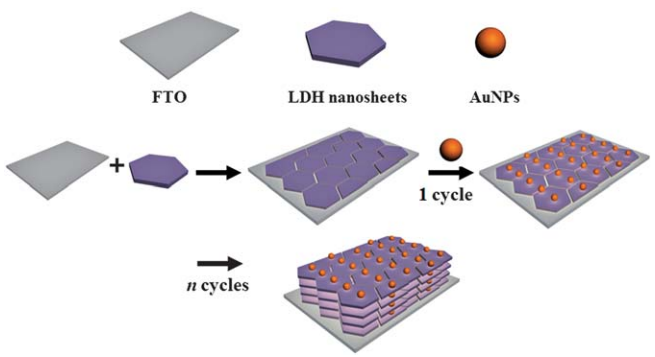

Scheme 1 Schematic representation for the assembly process of the $(LDH/AuNPs)_n$ UTFs.

2.2 Synthesis of AuNPs and Zn-Al LDH nanosheets

The AuNPs were synthesized by citrate reduction of aqueous $HAuCl_4$ at ~100 °C.[15] The synthesis of ZnAl-CO_3 LDH was similar to that described by Sasaki *et al.*[14a] In brief, $ZnCl_2 \cdot 6H_2O$ (0.010 mol), $AlCl_3 \cdot 9H_2O$ (0.005 mol) and urea (0.035 mol) were dissolved in aqueous solution (1 L), and it was stirred in a beaker at 100 °C for 2 days. The solid product was washed with water and dried in air at 60 °C. ZnAl-NO_3 LDH was prepared by the salt-acid method reported previously.[12d] The ZnAl-CO_3 LDH (1.0 g) was treated with aqueous salt-acid solution (1 L) containing HNO_3 (0.005 mol) and $NaNO_3$ (1.5 mol) in a flask under nitrogen flow and continuous stirring at ambient temperature for 24 h. The resulting ZnAl-NO_3 LDH was filtered, washed and vacuum-dried. Subsequently, a 0.1 g of ZnAl-NO_3 LDH was vigorously agitated in a 100 mL of formamide under N_2 flow at room temperature for 48 h. A colloidal suspension of positively charged ZnAl-LDH nanosheets was obtained (1 mg mL^{-1}) and used directly for the assembly of multilayer films.

2.3 Fabrication of LDH/AuNPs multilayer films

FTO substrates (exposed geometry area 1.5 cm^2) were cleaned in turn in an ultrasonic bath containing soapy water, deionized water, acetone, ethanol and deionized water for 10 min each, and then immersed in saturated NaOH aqueous solution for 20 min. After these procedures, the LBL assembly was performed by sequential dipping of FTO substrates in positively charged LDH nanosheets and negatively charged AuNPs colloidal suspension for 10 min each, followed by thorough rinsing with deionized water. The resulting films were dried in a vacuum oven at ambient temperature and are referred to as $(LDH/AuNPs)_n$. As comparison samples, the $(LDH/PSS/LDH/AuNPs)_n$ UTFs were performed by a similar assembly procedure in a sequence of LDH nanosheets, PSS (1 mg mL^{-1}), LDH nanosheets and AuNPs aqueous solution. The AuNPs modified FTO (AuNPs/FTO) and LDH modified FTO (LDH/FTO) were respectively prepared by dropping 50 μL of AuNPs colloid suspension or 50 μL of LDH nanosheets colloid suspension onto the FTO surface and dried in a vacuum oven at ambient temperature.

2.4 Characterizations and amperometric measurements

UV-vis absorption spectra were collected using a Shimadzu UV-2501PC spectrometer. X-Ray diffraction (XRD) patterns were recorded by a Rigaku XRD-6000 diffractometer, using Cu-Kα radiation (0.15418 nm) at 40 kV, 30 mA. The morphology of thin films was investigated using a scanning electron microscope (SEM Hitachi S-4700) with the accelerating voltage of 20 kV and a NanoScope IIIa atomic force microscope (AFM) from Veeco Instruments. TEM images were recorded on a JEOL JEM-2100 transmission electron microscope with the accelerating voltage of 200 kV. TEM grids of AuNPs and LBL films were prepared on a 300 mesh lacey carbon-coated copper grids and dried in air before imaging.

A CHI 660B electrochemical workstation (Shanghai Chenhua Instrument Co., China) was utilized for electrochemical measurements. A conventional three-electrode cell was used with a saturated Ag/AgCl electrode as the reference, a platinum wire as the counter, and the modified FTO electrode as the working electrode. Electrochemical impedance spectroscopy (EIS) dispersions were recorded with the frequency range from 0.01 Hz to 100 kHz in a 0.1 M KNO_3 with 1 mM $Fe(CN)_6^{4-/3-}$ or $Ru(NH_3)_6^{2+/3+}$solution at a potential of +0.21 V or −0.20 V *vs.* Ag/AgCl. The solutions were purged with highly purified nitrogen for 20 min prior to measurement. All measurements were performed at room temperature.

3. Results and discussion

3.1 Characterization of AuNPs and LDH nanosheets

The synthesized spherical citric-capped AuNPs present a typical single-particle plasmon resonance absorption band at 520 nm due to the collective oscillation of the electrons in the conduction band of the Au atoms under optical excitation (Fig. 1A), which is in agreement with the values reported for small size particles of *ca.* 14–20 nm.[15] The well-dispersed colloidal suspension was transparent and stable without any precipitation when stored at room temperature for more than two months, as shown in the inset of Fig. 1A. The TEM image of AuNPs is displayed in Fig. 1B, from which it is observed that the as-prepared AuNPs are of high quality in terms of size and uniformity. The size distribution histogram shows that the diameter of the AuNPs is 14 ± 2 nm (Fig. 1C). Fig. S1† displays the tapping-mode AFM image of the AuNPs deposited on a Si wafer substrate. The height profile measurement along the marked white line indicates that the average particle size is ~13.8 nm, which confirms the TEM result.

The XRD patterns of the synthesized ZnAl-CO_3 LDH and ZnAl-NO_3 LDH are displayed in Fig. 2A, all of which can be indexed to a rhombohedral structure (LDH) with 2θ 11.41° (d_{003} = 7.54 Å) for ZnAl-CO_3 LDH and 2θ 9.82° (d_{003} = 8.95 Å) for ZnAl-NO_3. No other crystalline phase was detected, indicating the formation of a well-crystallized hydrotalcite-like LDH phase. A typical SEM image (Fig. 2B) reveals that the sample of ZnAl-CO_3 LDH displays a hexagonal plate-like morphology with a mean lateral dimension of 3~5 μm. The TEM image (Fig. 2C) shows a thin platelet of morphologically irregular LDH nanosheet with a lateral size of 1~2 μm. A clear Tyndall light scattering effect was observed for the LDH nanosheets sol by a side-incident light beam (Fig. 2D), and the well-dispersed colloidal suspension is transparent and can be stored for more than one month.

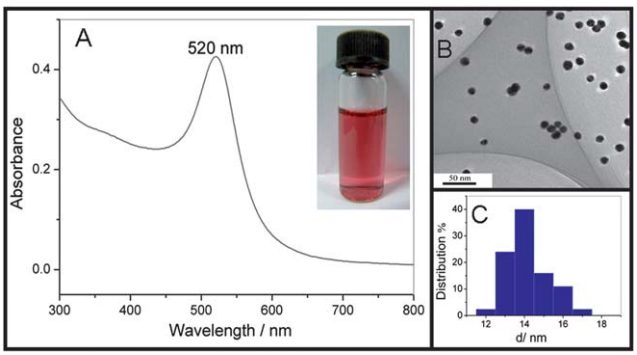

Fig. 1 (A) UV-vis spectrum of the colloidal AuNPs suspension (inset: digital photograph). (B) TEM image of the AuNPs. (C) Size distribution histogram of the AuNPs.

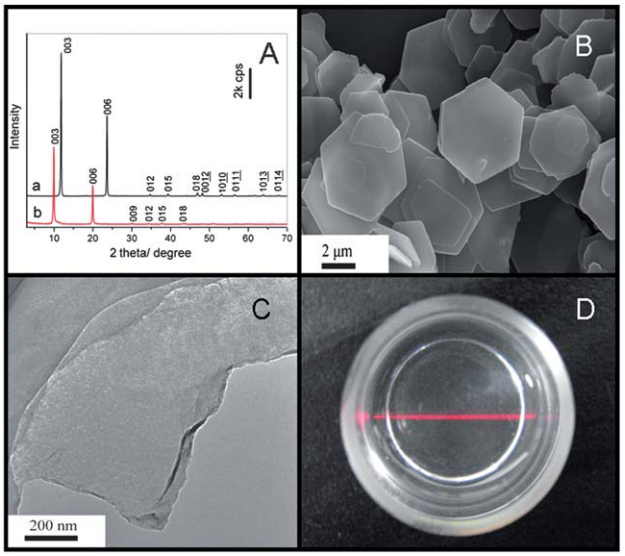

Fig. 2 (A) XRD patterns of (a) the ZnAl-CO_3 LDH, (b) the ZnAl-NO_3 LDH. (B) SEM image of the ZnAl-CO_3 LDH. (C) TEM image of the LDH nanosheets. (D) Digital photograph of a colloidal suspension of LDH nanosheets.

3.2 Assembly of the $(LDH/AuNPs)_n$ UTFs

The frequency of the surface plasmon resonance is significantly affected by electron interactions of the AuNPs through changing the environment and the level of the nanoparticles aggregation.[16] The film fabrication process of the resulting $(LDH/AuNPs)_n$ UTFs by alternate deposition of LDH nanosheets and AuNPs was monitored by UV-vis absorption spectroscopy as depicted in Fig. 3A. The strong absorption band at 520 nm originating from the plasmon resonance of individual AuNPs linearly correlates with the bilayer number n (inset of Fig. 3A), indicating a stepwise and regular film growth procedure. This is further confirmed by the visible color evolution with the increase of n (Fig. 3B).

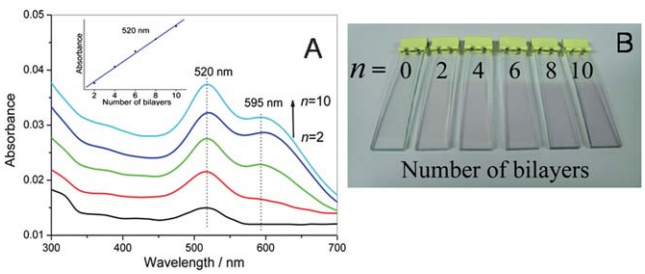

Fig. 3 (A) UV-vis spectra of the $(LDH/AuNPs)_n$ (n = 2–10) UTFs (inset: the linear relationship between absorbance at 520 nm and bilayer number n). (B) Digital photograph of the $(LDH/AuNPs)_n$ UTFs.

Importantly, a new band appearing at ~595 nm was observed as $n = 6$ and its intensity enhances upon increasing the bilayer number, which is associated with the interparticle plasmon coupling resonance of AuNPs that strongly depends on the distance/diameter ratio.[17]

The appearance of the band at ~595 nm results from two possibilities: the plasmon coupling resonance of AuNPs from one layer (intralayer) and from adjacent layers (interlayer). To further identify this point, a comparison study was carried out by separating AuNPs layers with a thicker spacing. This was accomplished by arranging an additional polyelectrolyte/clay (PSS/LDH) bilayer between adjacent LDH/AuNPs bilayers as a nanoscale spacer. As a result, the layered stacks with a repeat unit of (LDH/PSS/LDH/AuNPs) were prepared and the UV-vis spectra are shown in Fig. 4. It clearly shows that the increase in distance between adjacent AuNPs layers reduces the electronic interactions and the new band at 595 nm was therefore suppressed. The results reveal that the band at 595 nm for the $(LDH/AuNPs)_n$ UTFs mainly originates from the interlayer plasmon coupling. In addition, the slight red-shift of the plasmon maximum absorbance in Fig. 4 upon increasing n is related to the change in dielectric environment, which has been normally observed for the AuNPs coated with polymer layers or dissolved in different solvents.[18]

3.3 The structural and morphological study of the $(LDH/AuNPs)_n$ UTFs

The XRD patterns (Fig. 5A) of the $(LDH/AuNPs)_n$ UTFs were recorded in order to study the periodic structure. The increasing intensity of the reflection at about $2\theta = 0.62°$ upon increasing the deposition cycle indicates that the $(LDH/AuNPs)_n$ UTFs possess an ordered periodic structure in the direction normal to the substrate with a period of *ca.* 14.23 nm, which is close to that of the monolayer arrangement model of the $(LDH/AuNPs)_n$ system (0.48 nm for a LDH nanosheet and 14 nm for the average size of AuNPs). Fig. S2† illustrates the linear correlation of thickness of the $(LDH/AuNPs)_n$ UTFs as a function of n, from which the thickness augment per bilayer was observed to be ~14.5 nm. This is in accordance with the XRD results. The morphological feature of the UTFs was characterized by SEM and TEM images. A highly homogeneous and discrete distribution of dark

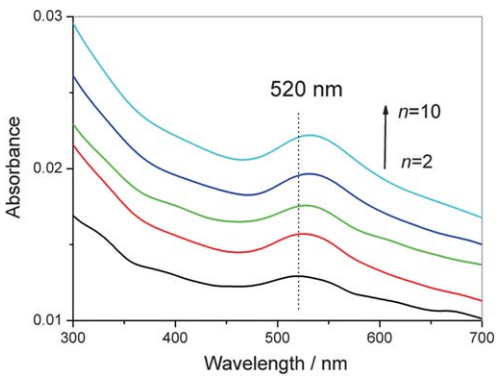

Fig. 4 UV-vis spectra of the $(LDH/PSS/LDH/AuNPs)_n$ (n = 2–10) UTFs.

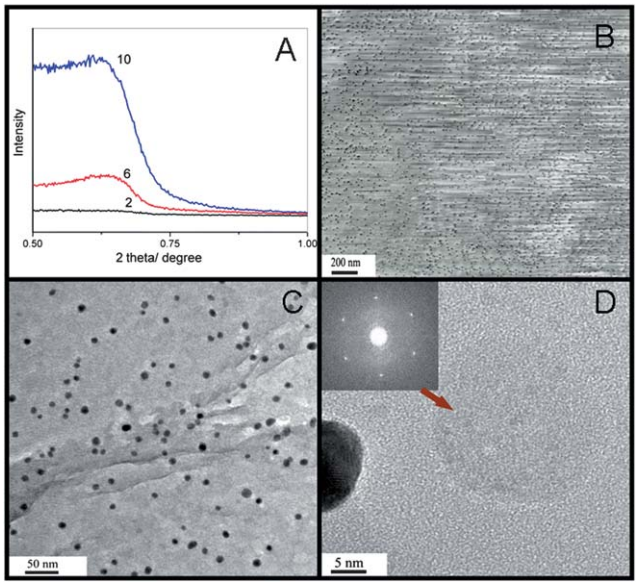

Fig. 5 (A) XRD patterns of the $(LDH/AuNPs)_n$ UTFs ($n = 2$, 6 and 10). (B) Top-view SEM image of the $(LDH/AuNPs)_8$ UTF. (C) TEM image of the $(LDH/AuNPs)_8$ UTF. (D) TEM image and the corresponding SAED pattern (inset) of the LDH nanosheets.

spherical spots corresponding to isolated AuNPs is clearly observed in the SEM image of the $(LDH/AuNPs)_8$ UTF (Fig. 5B). The TEM image (Fig. 5C) confirms that the AuNPs are immobilized on the surface of the LDH nanosheets and no aggregation or fusing into larger particles is observed. Moreover, the SAED (selected-area electron diffraction) pattern (Fig. 5D, inset) of the LDH nanosheets exhibits hexagonally arranged spots, indicating that the single-crystal structure of the LDH layer is stable even after exfoliation and LBL deposition.[13d,14a] The attenuated total reflection (ATR) FTIR spectra were also recorded in order to study the interlayer interactions. The spectrum of citric-capped AuNPs (Fig. S3,† curve a) shows two strong peaks centered at 1591 and 1394 cm^{-1} which can be attributed to the asymmetric and symmetric stretching vibrations of the COO^- group ($\nu_{as}(COO^-)$ and $\nu_s(COO^-)$) respectively;[24e] while the $\nu_{as}(COO^-)$ shifts to a higher frequency (from 1591 to 1605 cm^{-1}) in the case of the $(LDH/AuNPs)_8$ UTF (Fig. S3,† curve b), indicating the electrostatic interaction between the positively charged LDH layer and the negatively charged AuNPs.[12k]

The deposition process of the $(LDH/AuNPs)_n$ UTFs was further monitored by AFM (Fig. S4† and Fig. 6). The AFM topographical image of the $(LDH/AuNPs)_1$ UTF shows that the AuNPs are monodispersive with a root-mean-square (RMS) roughness of 3.254 nm (Fig. S4-A); LDH nanosheets can be observed after one subsequent deposition accompanied with a small increase in RMS (3.514 nm, Fig. S4-B and C). Fig. 6 illustrates that successive LBL deposition leads to a slight increase in RMS of the UTFs without substantial aggregation. These observations indicate that the positively charged LDH nanosheets with a rigid and crystalline structure provide an electrostatically-driven surface for anchoring and dispersing of AuNPs. This behavior is rather different from that in the AuNPs/organic cross-linker films wherein the particles

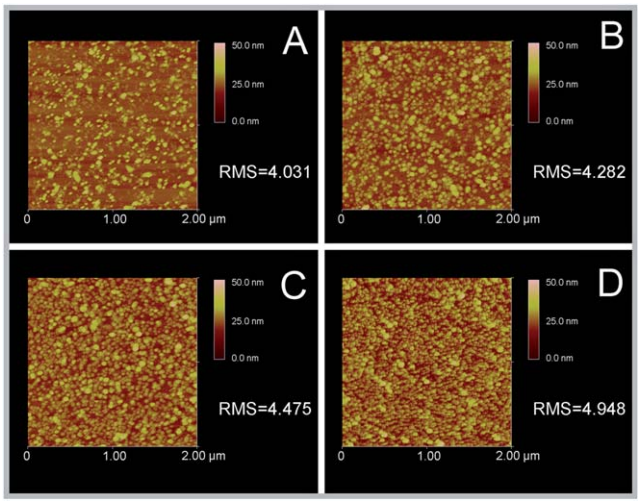

Fig. 6 Tapping-mode AFM images of the (A) $(LDH/AuNPs)_4$, (B) $(LDH/AuNPs)_6$, (C) $(LDH/AuNPs)_8$ and (D) $(LDH/AuNPs)_{10}$ UTF. The scan size for each image is 2 μm × 2 μm.

agglomerated to form larger clusters upon increasing the assembly bilayers.[4b,9a,17b,27d]

3.4 Electrochemical properties of the $(LDH/AuNPs)_n$ UTFs

The redox behavior of an electroactive species such as the negatively charged $Fe(CN)_6^{4-/3-}$ couple and the positively charged $Ru(NH_3)_6^{3+/2+}$ couple is a valuable and convenient tool for testing the kinetic barrier of the modified electrode, because electron transfer between the solution species and the electrode occurs by tunneling either through the barrier or through pores in the barrier.[19] Fig. 7 shows the cyclic voltammograms (CVs) of bare FTO, LDH/FTO, AuNPs/FTO, $(LDH/PSS/LDH/AuNPs)_8$/FTO and $(LDH/AuNPs)_8$/FTO electrode in 0.1 M KNO_3 solution containing 1 mM $Fe(CN)_6^{4-}$. A well-defined cyclic voltammetric (CV) characteristic of a diffusion-controlled redox process was observed at the bare FTO with a peak separation (ΔE_p) of 158 mV. However, the CV curve becomes

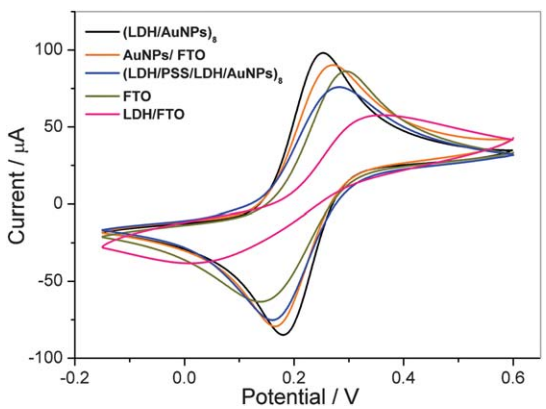

Fig. 7 Cyclic voltammograms of bare FTO, LDH/FTO, AuNPs/FTO, $(LDH/PSS/LDH/AuNPs)_8$/FTO and $(LDH/AuNPs)_8$/FTO electrode in 0.1 M KNO_3 solution containing 1 mM $Fe(CN)_6^{4-}$ at a scan rate of 20 mV s^{-1}.

distorted with a great decrease in peak currents at the LDH/FTO electrode, implying that the modification of the LDH nanosheets leads to a strong inhibition of electron transfer. As the immobilization of AuNPs on the electrode dramatically affects the electron transfer dynamics,[20] a more reversible CV response was noticed for the three AuNPs-based electrodes. Compared with the AuNPs/FTO and the $(LDH/PSS/LDH/AuNPs)_8$/FTO, the $(LDH/AuNPs)_8$/FTO exhibits an observable decrease in ΔE_p value (72 mV) accompanied with an increase in the peak currents, which suggests that the probe is able to diffuse through the LDH/AuNPs multilayers and undergoes a faster electron transfer at the electrode surface. The good electrical communication was further confirmed by a similar behavior in the solution containing $Ru(NH_3)_6^{3+}$ (Fig. S5†), indicating the generality of enhancement in electron transfer of redox probes at the $(LDH/AuNPs)_8$/FTO electrode.

Electrochemical impedance spectroscopy (EIS) is a useful method on the interface property of surface-modified electrodes and has been successfully used to characterize the formation of multilayer films on different substrates.[21] To obtain detailed information about the electrode/electrolyte interface, the impedance data were analyzed by using Randles equivalent circuit (inset of Fig. 8A). The EIS response consists of the linear portion at lower frequencies corresponding to the diffusion-limited process and the semicircle part at higher frequencies representing the electron-transfer-limited process.[22] The Nyquist plots of the bare and modified FTO electrodes are presented in Fig. 8A. The R_{ct} (the charge transfer resistance) value tested in $Fe(CN)_6^{4-/3-}$ solution can be obtained by measuring the diameter of the semicircle *via* simulation, which shows a sequence of $(LDH/AuNPs)_8$/FTO (12.8 Ω) < AuNPs/FTO (44.9 Ω) < $(LDH/PSS/LDH/AuNPs)_8$/FTO (191.8 Ω) < bare FTO (322.3 Ω) < LDH/FTO (1110 Ω). A same sequence was found when the positively charged $Ru(NH_3)_6^{3+/2+}$ redox probe was used (Fig. S6†). This is consistent with their CV behavior shown in Fig. 7 and Fig. S5,† further confirming that the modification of the electrode with the array of $(LDH/AuNPs)_n$ dramatically facilitates the electron transfer process regardless of the charge state of the redox probe. Furthermore, the influence of the bilayer number on the EIS response was also studied. Fig. 8B shows that the R_{ct} value decreases gradually upon increasing n (n varies from 2 to 8); while it turns to increase with further increasing the bilayer number (from 8 to 10) due to the blocking effect of LDH nanosheets in a thicker film.

Long range electron transfer reactions between AuNPs and the electrode surface separated by monolayer or multilayer films have been recently observed.[23] Interparticle interaction of AuNPs in an electromagnetic field alters the plasmon absorption greatly: if the quantum mechanical wave function overlap between adjacent particles occurs, the electron density will build up in the less shielded region between neighboring metallic cores. The plasmon frequency increases with the increase of electron density in a AuNP, resulting in the enhancement of plasmon absorption.[24] In the present study, it is proposed that the enhancement of interlayer plasmon coupling in the $(LDH/AuNPs)_n$ UTFs gives rise to the formation of electron tunneling junctions between adjacent AuNPs layers, which provides new channels for facilitating electron transfer throughout the multilayers. This is confirmed by the appearance of the UV-vis

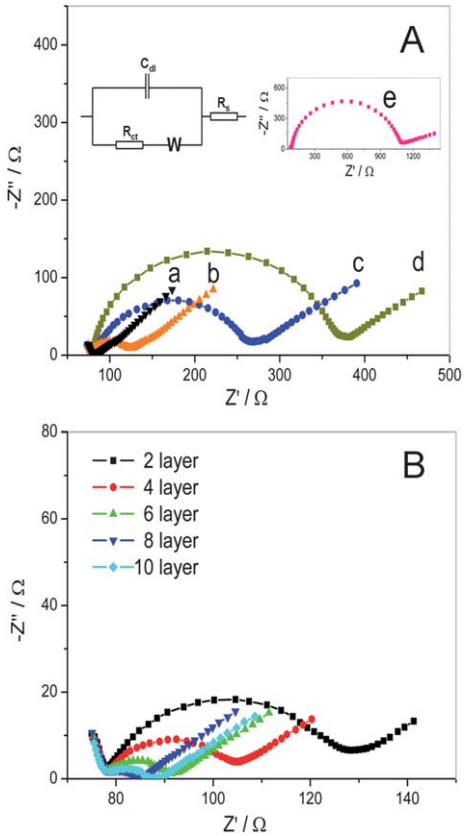

Fig. 8 (A) Nyquist plots of EIS for the (a) $(LDH/AuNPs)_8$/FTO, (b) AuNPs/FTO, (c) $(LDH/PSS/LDH/AuNPs)_8$/FTO, (d) bare FTO and (e) LDH/FTO. The Randles circuit is shown in the inset. (B) Nyquist plots of EIS for the $(LDH/AuNPs)_n$/FTO with various bilayer numbers ($n = 2$, 4, 6, 8 and 10) in 0.1 M KNO_3 solution containing 1 mM $Fe(CN)_6^{4-/3-}$ at a potential of +0.21 V *vs.* Ag/AgCl.

absorption at ~595 nm corresponding to the interparticle plasmon coupling resonance of AuNPs (Fig. 3A). In addition, compared with the AuNPs/FTO, the improved electrochemical performance of the $(LDH/AuNPs)_n$/FTO is associated with the high dispersion of AuNPs as well as the suitable microenvironment imposed by the LDH nanosheets. In contrast, for the $(LDH/PSS/LDH/AuNPs)_n$/FTO, the existence of additional inert spacer suppresses the interlayer plasmon coupling as evidenced by the disappearance of the band at 595 nm (Fig. 4), making AuNPs become inactive.

3.5 Electrocatalytic oxidation of glucose

The CV measurements of bare FTO, LDH/FTO, AuNPs/FTO, $(LDH/PSS/LDH/AuNPs)_8$/FTO and $(LDH/AuNPs)_8$/FTO electrode were carried out in a 0.1 M NaOH solution in the absence of glucose (Fig. 9). Compared with bare FTO and the LDH/FTO (curves d and e), the $(LDH/AuNPs)_8$/FTO gives one broad oxidation peak in the potential range 0.36–0.44 V and one distinct reduction peak at approximately 0.10 V (curve a), which correspond to the redox process of AuNPs, according to the following reaction:[25]

$$Au + OH^- - me^- \Leftrightarrow Au_2O_3 \cdot nH_2O \quad (1)$$

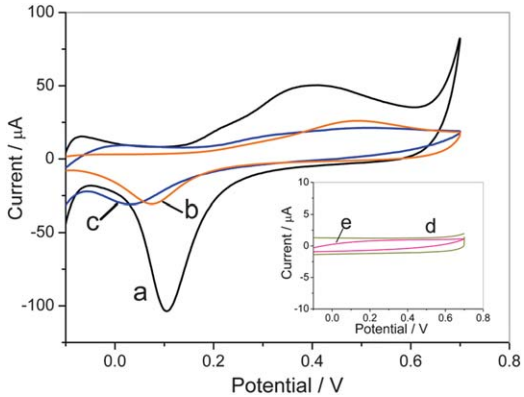

Fig. 9 CVs of the (a) $(LDH/AuNPs)_8$/FTO, (b) AuNPs/FTO, (c) $(LDH/PSS/LDH/AuNPs)_8$/FTO, (d) bare FTO, (e) LDH/FTO in 0.1 M NaOH at 50 mV s^{-1}.

Compared with the $(LDH/AuNPs)_8$/FTO electrode, the AuNPs/FTO and $(LDH/PSS/LDH/AuNPs)_8$/FTO also show CV behavior with much lower currents and larger ΔE_p value (curves b and c). These results indicate that the array of $(LDH/AuNPs)_n$ UTFs with single intervening LDH layers provides a confined and stable microenvironment for the accommodation of AuNPs and thus enhances the direct electrochemistry of AuNPs.

Fig. 10A shows the electrocatalytic activity towards the oxidation of glucose at the bare and modified FTO electrodes. No current response is observed at the bare FTO and LDH/FTO electrode (curves d and e); both the AuNPs/FTO and $(LDH/PSS/LDH/AuNPs)_8$/FTO show no marked electrocatalytic activity towards glucose as evidenced by the barely observable peaks (curves b and c). As expected, the $(LDH/AuNPs)_8$/FTO exhibits significant sharpening of the anodic peaks both in the anodic and cathodic scan as a consequence of the increased electroactivity of AuNPs (curve a). This indicates that the $(LDH/AuNPs)_n$ UTFs not only achieve a facile electron transfer process, but also electrocatalyze the oxidation of glucose efficiently. The anodic peak at 0.18 V presents the direct oxidation process of glucose. A rapid inhibition of the oxidation reaction occurs at higher potential corresponding to the formation of gold oxide which competes for surface adsorption sites with glucose. During the negative potential sweep, glucose can adsorb again and get oxidized as soon as the Au surface becomes free from oxide, resulting in the large cathodic reoxidation peak at 0.08 V.[26,8a] The dependence of electrochemical response on the bilayer number of the $(LDH/AuNPs)_n$ UTFs is depicted in Fig. 10B, from which the reoxidation current shows a systematic enhancement as n increases from 2 to 8; while a decrease in peak current was observed with further increasing the bilayer number. This inflection point at $n = 8$ agrees well with the lowest R_{ct} for the EIS spectrum of the $(LDH/AuNPs)_8$/FTO (shown in Fig. 8B). Therefore, the $(LDH/AuNPs)_8$/FTO was chosen as the optimum electrode for the voltammetric determination of glucose.

The determination of glucose at the $(LDH/AuNPs)_8$ modified electrode was performed with CV measurements. The cathodic reoxidation peak current of glucose was selected as the analytical signal (Fig. 11A and B). The results show that the peak current is proportional to the glucose concentration ranging from 50 μM to 20 mM (inset of Fig. 11B). The calibration equation can be

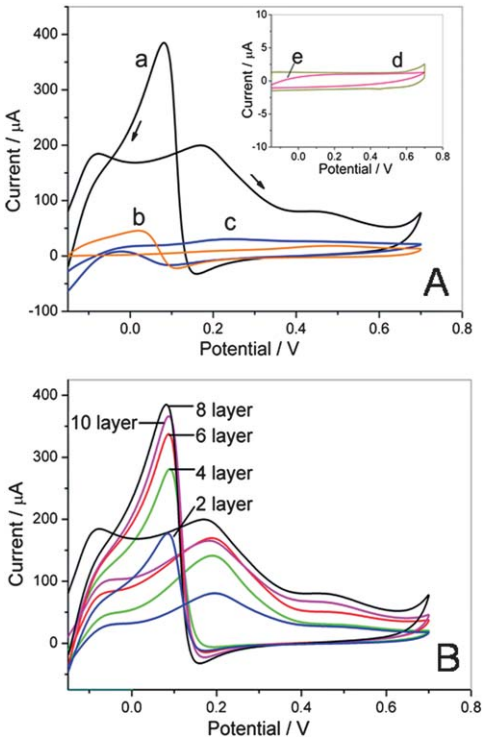

Fig. 10 (A) CVs for the oxidation of glucose (1 mM) at the (a) (LDH/AuNPs)$_8$/FTO, (b) AuNPs/FTO, (c) (LDH/PSS/LDH/AuNPs)$_8$/FTO, (d) bare FTO, (e) LDH/FTO. (B) CVs for the oxidation of glucose (1 mM) at the (LDH/AuNPs)$_n$/FTO with various bilayer number ($n = 2$, 4, 6, 8 and 10) in 0.1 M NaOH at 50 mV s^{-1}.

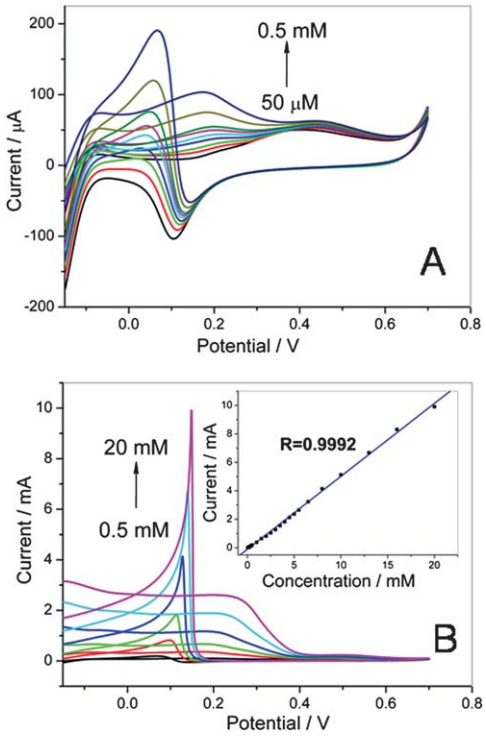

Fig. 11 CVs of the (LDH/AuNPs)$_8$/FTO in 0.1 M NaOH containing different concentrations of glucose: (A) 0.05, 0.10, 0.15, 0.20, 0.25, 0.30, 0.35, 0.40 and 0.50 mM; (B) 0.5, 2, 4, 8, 13 and 20 mM. Scan rate: 50 mV s^{-1} (inset: calibration curve of catalytic current *vs.* glucose concentration).

expressed as i (μA) = −106.7 + 512.3c (mM), with a correlation coefficient of 0.9992. The detection limit was estimated to be 10.8 μM (S/N = 3), which is lower than that of the reported AuNPs-based glucose sensors.[27] In view of the physiological level of glucose (3–8 mM), the linear concentration range (50 μM–20 mM) meets the requirement for clinical application. In addition, the sensitivity of the sensor was calculated to be 343 μA mM^{-1} cm^{-2}, which is much higher than those previously reported.[27] The results above demonstrate a high electrocatalytic activity and a broad linear response range for the (LDH/AuNPs)$_8$ modified electrode, which can be potentially used for practical applications.

The relative standard deviation (RSD) of the current response towards 1 mM glucose was 2.9% for 10 successive measurements. The long-term stability of the electrode was tested in 1 mM glucose solution using the same electrode for seven times each day over a continuous five-day period; the multilayer film retains 92% of its initial current response, indicating that the LDH matrix effectively stabilizes the AuNPs. Moreover, five electrodes were fabricated independently under the same conditions, which showed an acceptable reproducibility in 1 mM glucose solution with an RSD of 3.7%. The good stability and reproducibility in this work is due to the well-organized structure with the formation of highly dispersed AuNPs, illustrating the merits of inorganic LDH nanosheets as 2D building blocks for the immobilization of metal nanoparticles for electrochemical sensors.

4. Conclusions

In summary, we have successfully fabricated the LBL multilayers on FTO substrates containing AuNPs and LDH nanosheets driven by the electrostatic interaction between the two components. The structural and morphological studies indicate that the (LDH/AuNPs)$_n$ UTFs exhibit long range stacking order, in which the AuNPs are highly dispersed and immobilized with a monolayer arrangement in the LDH gallery. The resulting (LDH/AuNPs)$_n$ UTFs display improved electron transfer kinetics and excellent electrocatalytic activity towards glucose. Comparison studies demonstrate that the plasmon coupling of adjacent AuNPs layers in the (LDH/AuNPs)$_n$ UTFs plays a vital role in facilitating electron transfer across the multilayers. It is anticipated that the method in this work can be used to immobilize other metal or metal oxide nanoparticles within a 2D inorganic matrix for the fabrication of nano-scale sensors and electronic devices.

Acknowledgements

This project was supported by the 973 Program (Grant No.: 2011CBA00504), the National Natural Science Foundation of China, the 111 Project (Grant No.: B07004) and the Collaborative Project from the Beijing Education Committee.

Notes and references

1 F. Davis and S. P. J. Higson, *Biosens. Bioelectron.*, 2007, **22**, 1224.

2 S. Kerzenmacher, J. Ducrée, R. Zengerle and F. von Stetten, *J. Power Sources*, 2008, **1**, 182.
3 (*a*) Y. Wei, Y. Li, X. Liu, Y. Xian, G. Shi and L. Jin, *Biosens. Bioelectron.*, 2010, **26**, 275; (*b*) A. Heller and B. Feldman, *Chem. Rev.*, 2008, **108**, 2482.
4 (*a*) C. Shan, H. Yang, J. Song, D. Han, A. Ivaska and L. Niu, *Anal. Chem.*, 2009, **81**, 2378; (*b*) W. Yang, J. Wang, S. Zhao, Y. Sun and C. Sun, *Electrochem. Commun.*, 2006, **8**, 665; (*c*) X. Chu, B. Wu, C. Xiao, X. Zhang and J. Chen, *Electrochim. Acta*, 2010, **55**, 2848.
5 (*a*) L. Jiang and W. Zhang, *Biosens. Bioelectron.*, 2010, **25**, 1402; (*b*) J. Liu and D. Xue, *J. Mater. Chem.*, 2011, **21**, 223.
6 (*a*) S. Park, T. D. Chung and H. C. Kim, *Anal. Chem.*, 2003, **75**, 3046; (*b*) B. Beden, F. Largeaud, K. B. Kokoh and C. Lamy, *Electrochim. Acta*, 1996, **41**, 701.
7 (*a*) Y. P. Sun, H. Buck and T. E. Mallouk, *Anal. Chem.*, 2001, **73**, 1599; (*b*) Z. Liu, L. Huang, L. Zhang, H. Ma and Y. Ding, *Electrochim. Acta*, 2009, **54**, 7286; (*c*) R. Qiu, X. L. Zhang, R. Qiao, Y. Li, Y. I. Kim and Y. S. Kang, *Chem. Mater.*, 2007, **19**, 4174.
8 (*a*) M. Pasta, F. L. Mantia and Y. Cui, *Electrochim. Acta*, 2010, **55**, 5561; (*b*) C. Engelbrekt, K. H. Sørensen, J. Zhang, A. C. Welinder, P. S. Jensen and J. Ulstrup, *J. Mater. Chem.*, 2009, **19**, 7839; (*c*) T. Luczak, *Electrochim. Acta*, 2009, **54**, 5863; (*d*) H. Xu, L. Zeng, S. Xing, G. Shi, Y. Xian and L. Jin, *Electrochem. Commun.*, 2008, **10**, 1839.
9 (*a*) A. N. Shipway, M. Lahav and I. Willner, *Adv. Mater.*, 2000, **12**, 993; (*b*) M. Tominaga, T. Shimazoe, M. Nagashima and I. Taniguchi, *Chem. Lett.*, 2005, **34**, 202; (*c*) M. Tominaga, T. Shimazoe, M. Nagashima and I. Taniguchi, *Electrochem. Commun.*, 2005, **7**, 189; (*d*) J. Wang, W. Meng, X. Zheng, S. Liu and G. Li, *Biosens. Bioelectron.*, 2009, **24**, 1598; (*e*) Z. Wang and L. Ma, *Coord. Chem. Rev.*, 2009, **253**, 1607.
10 (*a*) T. Wang, X. Hu and S. Dong, *J. Mater. Chem.*, 2007, **17**, 4189; (*b*) J. Kim, S. W. Lee, P. T. Hammond and Y. Shao-Horn, *Chem. Mater.*, 2009, **21**, 2993; (*c*) W. Cheng, S. Dong and E. Wang, *J. Phys. Chem. B*, 2004, **108**, 19146.
11 (*a*) R. Toledano and D. Mandler, *Chem. Mater.*, 2010, **22**, 3943; (*b*) K. K. R. Datta, B. V. S. Reddy, K. Ariga and A. Vinu, *Angew. Chem., Int. Ed.*, 2010, **49**, 5961; (*c*) Y. Kobayashi, M. A. Correa-Duarte and L. M. Liz-Marzán, *Langmuir*, 2001, **17**, 6375.
12 (*a*) B. Monteiro, S. Gago, F. A. A. Paz, R. Bilsborrow, I. S. Gonçalves and M. Pillinger, *Inorg. Chem.*, 2008, **47**, 8674; (*b*) G. R. Williams and D. O'Hare, *J. Mater. Chem.*, 2006, **16**, 3065; (*c*) J. Liu, X. Huang, Y. Li, K. M. Sulieman, X. He and F. Sun, *J. Phys. Chem. B*, 2006, **110**, 21865; (*d*) A. Illaik, C. Taviot-Guého, J. Lavis, S. Commereuc, V. Verney and F. Leroux, *Chem. Mater.*, 2008, **20**, 4854; (*e*) J. Y. Uan, J. K. Lin and Y. S. Yung, *J. Mater. Chem.*, 2010, **20**, 761; (*f*) A. M. Fogg, V. M. Green, H. G. Harvey and D. O'Hare, *Adv. Mater.*, 1999, **11**, 1466; (*g*) A. M. Fogg, A. J. Freij and G. M. Parkinson, *Chem. Mater.*, 2002, **14**, 232; (*h*) L. Guadagnini, A. Mignani, E. Scavetta and D. Tonelli, *Electrochim. Acta*, 2010, **55**, 1217; (*i*) G. R. Williams, T. G. Dunbar, A. J. Beer, A. M. Fogg and D. O'Hare, *J. Mater. Chem.*, 2006, **16**, 1231; (*j*) F. Leroux and C. Taviot-Guého, *J. Mater. Chem.*, 2005, **15**, 3628; (*k*) W. Shi, S. He, M. Wei, D. G. Evans and X. Duan, *Adv. Funct. Mater.*, 2010, **20**, 3856.
13 (*a*) E. Scavetta, S. Stipa and D. Tonelli, *Electrochem. Commun.*, 2007, **9**, 2838; (*b*) A. M. Fogg, J. S. Dunn, S. G. Shyu, D. R. Cary and D. O'Hare, *Chem. Mater.*, 1998, **10**, 351; (*c*) S. Gago, M. Pillinger, R. A. S. Ferreira, L. D. Carlos, T. M. Santos and I. S. Gonçalves, *Chem. Mater.*, 2005, **17**, 5803; (*d*) X. Zhao, F. Zhang, S. Xu, D. G. Evans and X. Duan, *Chem. Mater.*, 2010, **22**, 3933; (*e*) J. Bauer, P. Behrens, M. Speckbacher and H. Langhals, *Adv. Funct. Mater.*, 2003, **13**, 241; (*f*) S. Gago, T. Costa, J. S. de Melo, I. S. Gonçalves and M. Pillinger, *J. Mater. Chem.*, 2008, **18**, 894; (*g*) F. Leroux, A. Illaik, T. Stimpfling, A. Troutier-Thuilliez, S. Fleutot, H. Martinez, J. Cellier and V. Verney, *J. Mater. Chem.*, 2010, **20**, 9484; (*h*) G. G. Aloisi, U. Costantino, F. Elisei, L. Latterini, C. Natali and M. Nocchetti, *J. Mater. Chem.*, 2002, **12**, 3316; (*i*) H. Ai, X. Huang, Z. Zhu, J. Liu, Q. Chi, Y. Li, Z. Li and X. Ji, *Biosens. Bioelectron.*, 2008, **24**, 1048; (*j*) H. Yin, L. Cui, S. Ai, H. Fan and L. Zhu, *Electrochim. Acta*, 2010, **55**, 603; (*k*) Y. Zhao, M. Wei, J. Lu, Z. L. Wang and X. Duan, *ACS Nano*, 2009, **3**, 4009; (*l*) D. Yan, J. Lu, J. Ma, M. Wei, D. G. Evans and X. Duan, *Angew. Chem., Int. Ed.*, 2011, **50**, 720.
14 (*a*) Z. Liu, R. Ma, M. Osada, N. Iyi, Y. Ebina, K. Takada and T. Sasaki, *J. Am. Chem. Soc.*, 2006, **128**, 4872; (*b*) G. Abellán, E. Coronado, C. Martí-Gastaldo, E. Pinilla-Cienfuegos and A. Ribera, *J. Mater. Chem.*, 2010, **20**, 7451; (*c*) L. Li, R. Ma, Y. Ebina, N. Iyi and T. Sasaki, *Chem. Mater.*, 2005, **17**, 4386; (*d*) D. Yan, J. Lu, M. Wei, J. Han, J. Ma, F. Li, D. G. Evans and X. Duan, *Angew. Chem., Int. Ed.*, 2009, **48**, 3073; (*e*) T. Hibino and M. Kobayashi, *J. Mater. Chem.*, 2005, **15**, 653.
15 (*a*) J. Turkevich, P. C. Stevenson and J. Hillier, *Discuss. Faraday Soc.*, 1951, **11**, 55; (*b*) K. R. Brown, D. G. Walter and M. J. Natan, *Chem. Mater.*, 2000, **12**, 306; (*c*) J. Zhang, M. Kambyashi and M. Oyama, *Electrochem. Commun.*, 2004, **6**, 683; (*d*) V. C. Ferreira, A. F. Silva and L. M. Abrantes, *J. Phys. Chem. C*, 2010, **114**, 7710.
16 (*a*) J. H. Fendler, *Chem. Mater.*, 2001, **13**, 3196; (*b*) D. I. Gittins and F. Caruso, *J. Phys. Chem. B*, 2001, **105**, 6846; (*c*) C. Jiang, S. Markutsya and V. V. Tsukruk, *Langmuir*, 2004, **20**, 882; (*d*) H. Chen, X. Kou, Z. Yang, W. Ni and J. Wang, *Langmuir*, 2008, **24**, 5233.
17 (*a*) N. Sakai, T. Sasaki, K. Matsubara and T. Tatsuma, *J. Mater. Chem.*, 2010, **20**, 4371; (*b*) F. Zhang and M. P. Srinivasan, *J. Colloid Interface Sci.*, 2008, **319**, 450; (*c*) J. Schmitt, P. Machtle, D. Eck, H. Mohwald and C. A. Helm, *Langmuir*, 1999, **15**, 3256.
18 (*a*) N. Malikova, I. Pastoriza-Santos, M. Schierhorn, N. A. Kotov and L. M. Liz-Marán, *Langmuir*, 2002, **18**, 3694; (*b*) S. Vial, I. Pastoriza-Santos, J. Pérez-Juste and L. M. Liz-Marán, *Langmuir*, 2007, **26**, 4606; (*c*) K. S. Mayya, B. Schoeler and F. Caruso, *Adv. Funct. Mater.*, 2003, **13**, 183; (*d*) S. Huang, K. Minami, H. Sakaue, S. Shigubara and T. Takahagi, *J. Appl. Phys.*, 2002, **92**, 7486.
19 (*a*) G. Maduraiveeran and R. Ramaraj, *J. Electroanal. Chem.*, 2007, **608**, 52; (*b*) J. Jia, B. Wang, A. Wu, G. Cheng, Z. Li and S. Dong, *Anal. Chem.*, 2002, **74**, 2217; (*c*) H. Orikasa, T. Akahane, M. Okada, Y. Tong, J. Ozaki and T. Kyotani, *J. Mater. Chem.*, 2009, **19**, 4615; (*d*) S. Griveau, V. Albin, T. Pauporte, J. H. Zagal and F. Bedioui, *J. Mater. Chem.*, 2002, **12**, 225.
20 (*a*) J. Zhao, C. R. Bradbury, S. Huclova, I. Potapova, M. Carrara and D. J. Fermín, *J. Phys. Chem. B*, 2005, **109**, 22985; (*b*) K. Stolarczyk and R. Bilewicz, *Electrochim. Acta*, 2006, **51**, 2358.
21 (*a*) Y. Z. Zhang, H. Y. Ma, K. Y. Zhang, S. J. Zhang and J. Zhang, *Electrochim. Acta*, 2009, **54**, 2385; (*b*) D. H. Wu, Q. Zhang, X. Chu, H. B. Wang, G. L. Shen and R. Q. Yu, *Biosens. Bioelectron.*, 2010, **25**, 1025; (*c*) J. Pillay, K. I. Ozoemena, R. T. Tshikhudo and R. M. Moutloali, *Langmuir*, 2010, **26**, 9061; (*d*) B. Yu, H. Hu, D. Wang, W. T. S. Huck, F. Zhou and W. Liu, *J. Mater. Chem.*, 2009, **19**, 8129.
22 (*a*) B. Ballarin, M. C. Cassani, E. Scavetta and D. Tonelli, *Electrochim. Acta*, 2008, **53**, 8034; (*b*) A. J. Bard and L. R. Faulkner, *Electrochemical Methods: Fundamentals and Applications*, Wiley, New York, 1980.
23 (*a*) C. R. Raj, A. I. Abdelrahman and T. Ohsaka, *Electrochem. Commun.*, 2005, **7**, 888; (*b*) J. Zhao, C. R. Bradbury and D. J. Fermín, *J. Phys. Chem. C*, 2008, **112**, 6832; (*c*) F. Mirkhalaf and D. J. Schiffrin, *Langmuir*, 2010, **26**, 14995.
24 (*a*) T. Baum, D. Bethell, M. Brust and D. J. Schiffrin, *Langmuir*, 1999, **15**, 866; (*b*) J. Park, T. Momma and T. Osaka, *Electrochim. Acta*, 2007, **52**, 5914; (*c*) J. J. Shiang and J. R. Heath, *J. Phys. Chem. B*, 1998, **102**, 3425; (*d*) T. Sagara, N. Kato and N. Nakashima, *J. Phys. Chem. B*, 2002, **106**, 1205; (*e*) T. Wang, R. Zheng, X. Hu, L. Zhang and S. Dong, *J. Phys. Chem. B*, 2006, **110**, 14179.
25 (*a*) J. Luo, M. M. Maye, Y. Lou, L. Han, M. Hepel and C. J. Zhong, *Catal. Today*, 2002, **77**, 127; (*b*) K. A. Assiongbon and D. Roy, *Surf. Sci.*, 2005, **594**, 99.
26 (*a*) M. Tominage, T. Shimazoe, M. Nagashima, H. Kusuda, A. Kubo, Y. Kuwahara and I. Taniguchi, *J. Electroanal. Chem.*, 2006, **590**, 37; (*b*) P. Parpot, N. Nunes and A. P. Bettencourt, *J. Electroanal. Chem.*, 2006, **596**, 65; (*c*) S. B. Aoun, Z. Dursun, T. Koga, G. S. Bang, T. Sotomura and I. Taniguchi, *J. Electroanal. Chem.*, 2004, **567**, 175.
27 (*a*) Y. Li, Y. Song, C. Yang and X. Xia, *Electrochem. Commun.*, 2007, **9**, 981; (*b*) Y. J. Yang and S. Hu, *Electrochim. Acta*, 2010, **55**, 3471; (*c*) C. Shan, H. Yang, D. Han, Q. Zhang, A. Ivaska and L. Niu, *Biosens. Bioelectron.*, 2010, **25**, 1070; (*d*) F. Kurniawan, V. Tsakova and V. M. Mirsky, *Electroanalysis*, 2006, **18**, 1937; (*e*) F. Li, J. Song, F. Li, X. Wang, Q. Zhang, D. Han, A. Ivaska and L. Niu, *Biosens. Bioelectron.*, 2009, **25**, 883.